

## Reactions of Sulfur Dioxide with Neutral Vanadium Oxide Clusters in the Gas Phase. II. Experimental Study Employing Single-Photon Ionization

Sheng-Gui He,<sup>‡,†</sup> Yan Xie,<sup>†</sup> Feng Dong,<sup>‡,§</sup> Scott Heinbuch,<sup>§,||</sup> Elena Jakubikova,<sup>⊥,†</sup> J. J. Rocca,<sup>§,||</sup> and Elliot R. Bernstein<sup>\*,‡,§</sup>

Departments of Chemistry and Electrical and Computer Engineering, Colorado State University, Fort Collins, Colorado 80523-1872, and NSF ERC for Extreme Ultraviolet Science and Technology, Colorado State University, Fort Collins, Colorado 80523-1320

Received: June 30, 2008; Revised Manuscript Received: August 15, 2008

Single-photon ionization through vacuum ultraviolet (VUV, 10.5 eV) and soft X-ray (extreme ultraviolet, EUV, 26.5 eV) laser radiation is successfully employed for the study of the reactions of neutral vanadium oxide clusters ( $V_mO_n$ ) with sulfur dioxide ( $SO_2$ ) in the gas phase.  $V_mO_n$  clusters are generated by reaction of a laser-generated vanadium plasma with  $O_2$  in a supersonic expansion. The clusters are cooled in the expansion and are reacted with  $SO_2$  in a fast-flow reactor. Detection of neutral clusters and products is through ionization employing VUV and EUV laser radiation and time-of-flight mass spectrometry. Many association reaction intermediates [ $V_mO_nSO_2$  and  $V_2O_4(SO_2)_2$ ] are observed. Isolated SO is also observed, as a product as predicted by theoretical studies presented in part I (*J. Phys. Chem. A* **2007**, *111*, 13339). A weak feature at the  $SO_3$  mass channel (80 amu) is suggested to be present in the product mass spectra. Further reactions of the intermediates with  $O_2$  are positively identified for  $VO_2SO_2$ ,  $V_3O_7SO_2$ , and  $V_5O_{10}SO_2$ . Reaction mechanisms are interpreted on the basis of the observations and preliminary theoretical calculations. Molecular level reaction mechanisms for oxidation of  $SO_2$  to  $SO_3$  facilitated by condensed-phase vanadium oxides as catalysts are suggested.

### I. Introduction

Vanadium oxides are very important industrial heterogeneous catalysts.<sup>1–4</sup>  $V_2O_5$  catalysis has been employed for oxidation of  $SO_2$  to  $SO_3$  (sulfuric acid production,  $SO_2$  removal), selective reduction of  $NO_x$  with  $NH_3$ , oxidation of hydrocarbons (butene, benzene, *o*-xylene, and naphthalene) to anhydrides, and for other reactions. To improve efficiency of industrial catalysts and to find new catalysts for these important processes, fundamental studies of catalytic mechanisms are essential, especially with regard to microscopic or molecular level reaction dynamics and kinetics.<sup>5</sup> With the development of spectroscopic catalyst characterization techniques (X-ray absorption, infrared and Raman spectroscopy, and solid-state NMR, etc.), the understanding of catalytic mechanisms involving condensed-phase transition metal oxide systems<sup>6</sup> has increased. Nevertheless, only very limited observations for complex heterogeneous catalytic systems are presently available, and microscopic reaction mechanisms are sometimes proposed on the basis of incompletely supported models, ideas, and concepts. Oxidation of  $SO_2$  over supported vanadia catalysts has been carefully studied,<sup>7–9</sup> and conclusive mechanisms have been drawn based heavily on  $O=V-(O-support)_3$  structural models.<sup>3,4,6</sup> Very recent theoretical and experimental studies,<sup>10,11</sup> however, strongly suggest that the catalyst should possess an  $O_2O=V-O-support$  structure.

Gas-phase vanadium oxide clusters ( $V_mO_n$ ) are excellent model systems to help elucidate and understand molecular level processes occurring in the above-mentioned reactions using vanadia catalysts. Catalytically active sites can be simulated/ modeled by clusters with particular *m* and *n*: the difficulty is to find proper values from *m* and *n* that represent an active site.<sup>12–15</sup> One obvious advantage of using clusters to simulate catalytically active sites is that modern quantum chemistry calculations can be applied to obtain reliable information that is hard to access by direct observations.<sup>5</sup>

Successful joint experimental and theoretical studies of the reactivity of cationic  $V_mO_n$  toward hydrocarbons have been reported.<sup>16–20</sup> Many other experimental and theoretical investigations of vanadium oxide clusters are reported; brief reviews can be found in refs 19 and 21. Because electric and magnetic forces can be used to control and manipulate charged particles and charged particles can be detected very efficiently, most of the experimental studies are on cationic and anionic vanadium oxide clusters. To date, no report can be found for experimental reactivity studies of *neutral* vanadium (and other transition metal) oxide clusters. The major difficulty for such studies of the reactivity of neutral metal oxide clusters lies in finding a valid method to ionize neutral species with typical ionization energies in the range of 8–10 eV or higher (e.g.,  $VO_3$ ,  $SO_3$ ,  $N_2$ , and  $V_3O_8$ ,...), and in detecting them without loss of information (neutral cluster mass and abundance distributions). Typical multiphoton and electron impact ionization almost always cause severe cluster fragmentation and thus loss of original neutral cluster information.

Recently, single-photon ionization (SPI) through vacuum ultraviolet (VUV) and soft X-ray (EUV) laser radiation have been successfully used by us to study a series of neutral metal oxide cluster distributions without fragmentation.<sup>21–26</sup> The 118

\* To whom correspondence should be addressed.

<sup>†</sup> Department of Chemistry, Colorado State University.

<sup>‡</sup> Current address: State Key Laboratory for Structural Chemistry of Unstable and Stable Species, Institute of Chemistry, Chinese Academy of Sciences, Zhongguancun, Haidian, Beijing 100080, China.

<sup>§</sup> NSF ERC for Extreme Ultraviolet Science and Technology.

<sup>||</sup> Department of Electrical and Computer Engineering, Colorado State University.

<sup>⊥</sup> Current address: Theoretical Division, Los Alamos National Laboratory, Los Alamos, NM 87545.

nm single-photon energy is 10.5 eV, and the soft X-ray single-photon energy is 26.5 eV; for most transition metal oxide clusters ( $M_nO_n$ ,  $M = \text{Ti, V, Co, Nb, Fe, ...}$ ), the ionization energy is around 10 eV. Therefore, clusters ionized by X-ray laser radiation may have more excess energy than those ionized by 118 nm laser radiation. Thus, for X-ray laser ionization, the relative signal intensities of weakly bound products, such as association products,  $V_mO_n\text{SO}_2$ , can be smaller than those observed by 118 nm ionization, because more excess energy can remain in the clusters and the clusters can fragment. Consequentially, X-ray laser ionization has both pros and cons, but, nonetheless, it is clearly essential to detect all the neutral clusters and their products. The adoption of soft X-ray laser ionization for this study is important for detection of some products with high ionization energy (IE), such as  $\text{SO}_3$  and  $V_mO_n$  clusters that are oxygen-rich. We have employed 26.5 eV single-photon ionization to detect these clusters and products and report these results herein which are unique and essential to the demonstration of our conclusions.

In the present work, a fast-flow reactor<sup>27</sup> is further employed to study the reactivity of neutral vanadium oxide clusters toward  $\text{SO}_2$ . The motivation is to understand possible molecular level mechanisms for oxidation of  $\text{SO}_2$  in condensed-phase catalytic reactions. In the present work, the experimental results are reported and discussed on the basis of the observations and preliminary calculations. Details of the calculations are presented in the part I of this series.<sup>28</sup> On the basis of these results, full catalytic cycles for the condensed-phase systems are suggested.

## II. Experimental Procedures

The experimental setup for a pulsed laser ablation/supersonic nozzle coupled with a fast-flow reactor has been described in our previous study of methanol formation on metal clusters.<sup>29</sup> Only a brief outline of the experiments is given below.  $V_mO_n$  clusters are generated by laser ablation of vanadium metal foil in the presence of 1%  $\text{O}_2$  seeded in a He carrier gas. The gas is controlled by a pulsed nozzle (called nozzle I in this work) made by the R. M. Jordan Co. The clusters formed in a gas channel (i.d. 2 mm  $\times$  19 mm) are expanded and reacted with a  $\text{SO}_2$  or an  $\text{SO}_2/\text{O}_2$  mixture seeded or unseeded in He in a fast-flow reactor (i.d. 6 mm  $\times$  76 mm). The reactant gases ( $\text{SO}_2$  and  $\text{SO}_2/\text{O}_2$ , with or without He) are pulsed into the tube 20 mm downstream from the exit of the narrow cluster formation channel by a pulsed valve (General Valve Series 9, called nozzle II in this work). Reactions in the fast-flow reactor are believed to occur at near room temperature due to the large number of collisions between  $V_mO_n$  clusters and the bath gas (He) and/or reactants ( $\text{SO}_2$ ,  $\text{SO}_2/\text{O}_2$ ).<sup>27</sup> The instantaneous total reactant gas pressure in the reactor is about 14 Torr in the case in which the He bath gas is used. The ions are deflected from the molecular beam by an electric field located 5 mm downstream of the fast-flow reactor. The gases exiting the reactor are skimmed (i.d. 5 mm or i.d. 2 mm) into the vacuum system of a time-of-flight mass spectrometer (TOFMS) for ionization by radiation of one of two different lasers: a 118 nm (10.5 eV) VUV laser or a 46.9 nm (26.5 eV) soft X-ray laser. Ions are detected and signals are recorded as previously described.<sup>29,30</sup> The 118 nm laser light is generated by focusing the third harmonic (355 nm,  $\sim 30$  mJ/pulse) of a Nd:YAG laser in a tripling cell that contains about a 250 Torr argon/xenon (10/1) gas mixture. To separate the generated 118 nm laser beam from the 355 nm fundamental beam, a magnesium fluoride prism (made by Crystaltechno Ltd., Moscow, Russia; apex angle =  $6^\circ$ ), which was not employed in our previous studies,<sup>21–25</sup> is inserted into the laser beams. In

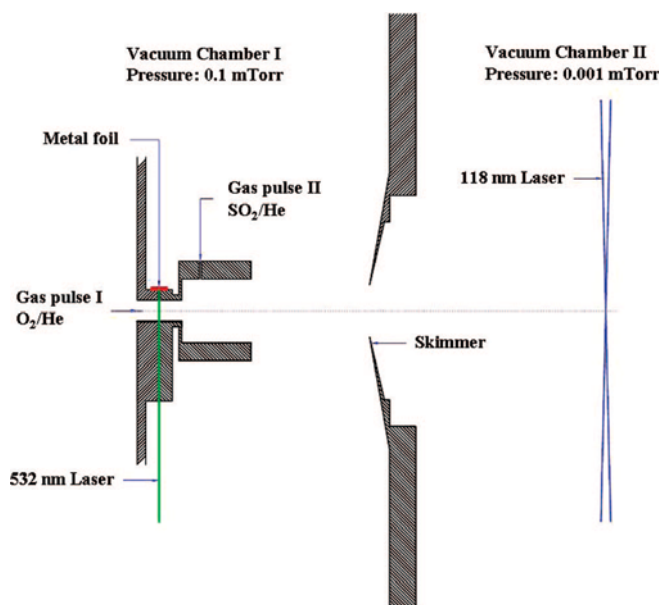


**Figure 1.** Schematic diagram of the experimental setup using 118 nm laser radiation as the ionization source.

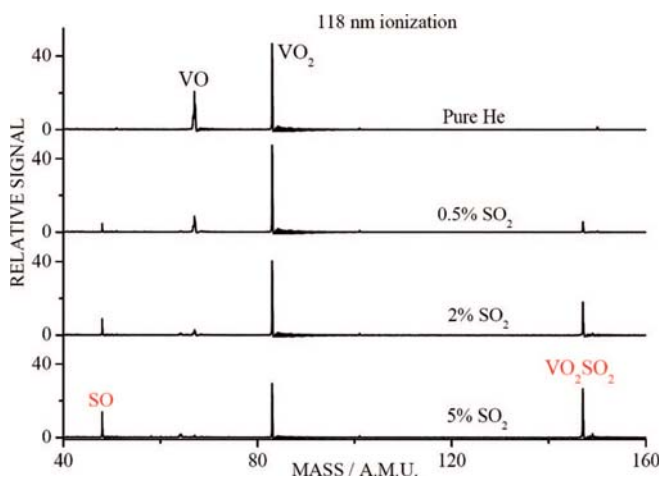
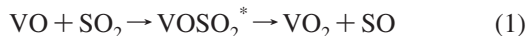


**Figure 2.** TOF mass spectra (low-mass region) for reactions of  $V_mO_n$  with different concentrations of  $\text{SO}_2$  seeded in He. The concentrations of  $\text{SO}_2$  are 0, 0.5, 2, and 5% from top to bottom traces. 1%  $\text{O}_2$  seeded in He is used to produce  $V_mO_n$  (this condition is kept to obtain all the TOF spectra reported in the present work).

this case, one is quite certain that the mass signals are generated by ionization purely through the VUV laser radiation with low power ( $\sim 1$   $\mu\text{J/pulse}$ , pulse duration  $\sim 5$  ns). The soft X-ray laser radiation ( $\sim 10$   $\mu\text{J/pulse}$ , pulse duration  $\sim 1.5$  ns) is generated from the  $3p(^1S_0) \rightarrow 3s(^1P_1)$  transition of Ne-like Ar: a detailed description of this laser can be found in the literature.<sup>31,32</sup> The fast-flow setup employing a 118 nm laser as an ionization source is schematically shown in Figure 1. The X-ray laser radiation is not focused in the TOFMS ionization region.

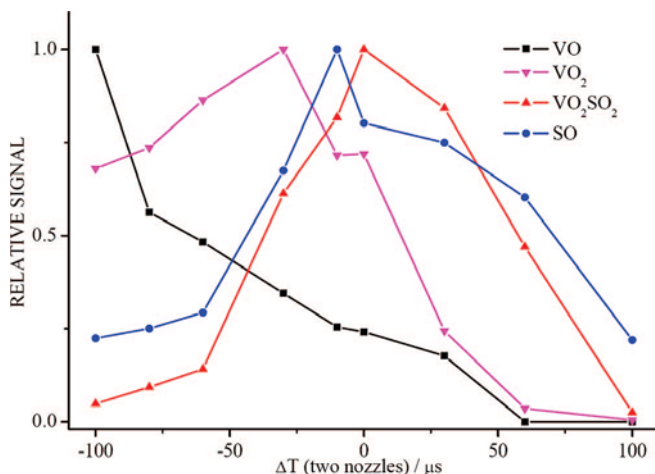
## III. Results

Figure 2 presents low-mass spectra for reactions of  $V_mO_n$  with different concentrations of  $\text{SO}_2$  seeded in He in the fast-flow reactor. Products  $\text{SO}$  and  $\text{VO}_2\text{SO}_2$  are observed through 118 nm single-photon ionization. The intensities of products ( $\text{SO}$  and  $\text{VO}_2\text{SO}_2$ ) increase, while the intensities of the reactant clusters ( $\text{VO}$  and  $\text{VO}_2$ ) decrease as  $\text{SO}_2$  concentrations increase. The following reactions can be derived:



in which  $VOSO_2^*$  and  $VO_2SO_2^*$  (or generally  $V_mO_nSO_2^*$ ) are initial association products that carry center of mass collision energy, reactant initial vibrational energy, and association energy, and  $VO_2SO_2$  (or generally  $V_mO_nSO_2$ ) is the product stabilized by collisions with He (or reactants). Only products containing transition metal/metal oxide clusters are detected in the previous neutral cluster studies,<sup>29,33</sup> and SO as an isolated product is observed in the reactions of neutral transition metal/metal oxide clusters for the first time in these experiments. The SO signal immediately disappears if the ablation laser is blocked, which indicates SO comes from the reaction of the  $V_mO_n$  with  $SO_2$ . Signals of products and reactants are dependent on the relative delay times for opening the two pulsed nozzles (I and II). Figure 3 gives the relative signal change of VO,  $VO_2$ , SO, and  $VO_2SO_2$  with the change of relative delay times ( $\Delta T$ ) between the openings of nozzles I and II. Nozzle II is always fired earlier than nozzle I to make sure the reactor is filled by the reactant gases before the clusters arrive. In the experiment,  $\Delta T \approx 0 \mu s$  corresponds to the condition for the best product yield; negative  $\Delta T$  values correspond to less overlap between the two gas pulses. The increase of  $VO_2$  signal with the increase of  $\Delta T$  at the beginning ( $\Delta T < -25 \mu s$ ) further verifies that reaction 1 happens in the reactor. The decrease of the product signal at large positive  $\Delta T$  values can be understood as too much mixing of the two gas pulses so that the clusters and products are diluted in space and/or time through collisional scattering. Note that the original laser ablation created  $V_mO_n$  clusters have a time distribution within only about  $10 \mu s$ . In the present work, the mass spectra are all obtained under the condition that products have a maximum signal, which corresponds to  $\Delta T \approx 0 \mu s$  in Figure 3.

Figures 4 and 5 plot high-mass spectra for reactions of  $V_mO_n$  with different concentrations of  $SO_2$  seeded in He. Many association products ( $V_mO_nSO_2$ ) are observed.  $V_2O_4SO_2$  further reacts with  $SO_2$  to form  $V_2O_4(SO_2)_2$  if high concentrations ( $\geq 5\%$ ) of  $SO_2$  are used. A careful comparison between the spectra indicates that for an oxygen series ( $V_mO_n$ ,  $m = \text{constant}$ ,



**Figure 3.** Relative signal change of VO (solid square),  $VO_2$  (solid down triangle),  $VO_2SO_2$  (solid up triangle), and SO (solid circle) with the change of relative delay times ( $\Delta T$ ) for opening two nozzles that deliver the two gas pulses discussed in the Experimental Procedures. 5%  $SO_2$  seeded in He is used for the reaction of  $V_mO_n$  with  $SO_2$ . See text for details.

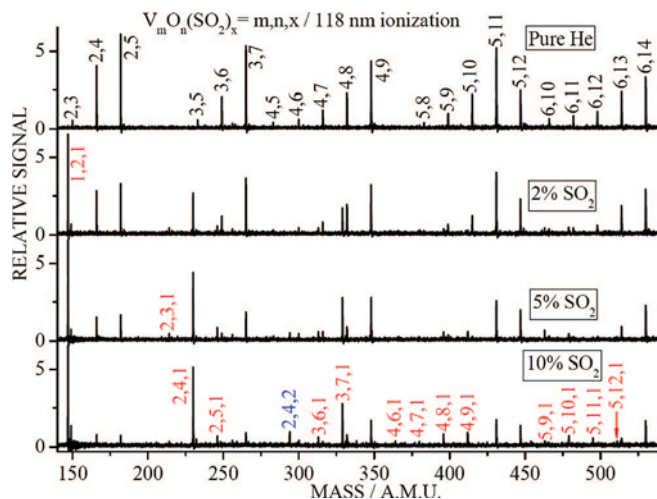


**Figure 4.** TOF mass spectra (high-mass region I) for reactions of  $V_mO_n$  with different concentrations of  $SO_2$  seeded in He. The concentrations of  $SO_2$  are 0, 2, 5, and 10% from top to bottom traces.

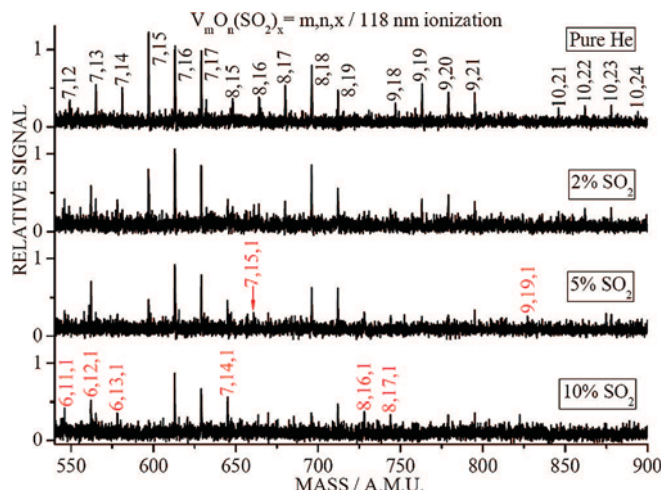


**Figure 5.** TOF mass spectra (high-mass region II) for reactions of  $V_mO_n$  with different concentrations of  $SO_2$  seeded in He. The concentrations of  $SO_2$  are 0, 2, 5, and 10% from top to bottom traces.

$n = \text{variable}$ ), clusters with lower  $n$  values usually have relatively higher depletion rates than clusters with higher  $n$  values (more oxygen-rich clusters); for example,  $V_3O_6$  vs  $V_3O_7$ ,  $V_4O_8$  vs  $V_4O_9$ ,  $V_5O_{10}$  vs  $V_5O_{12}$ ,  $V_6O_{13}$  vs  $V_6O_{14}$ ,  $V_7O_{15}$  vs  $V_7O_{16,17}$ , and  $V_8O_{17}$  vs  $V_8O_{18,19}$ . We may derive the following processes similar and parallel to reactions 1 and 2 on the basis of such observations:

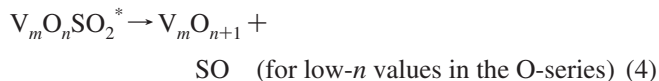
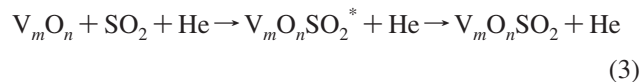
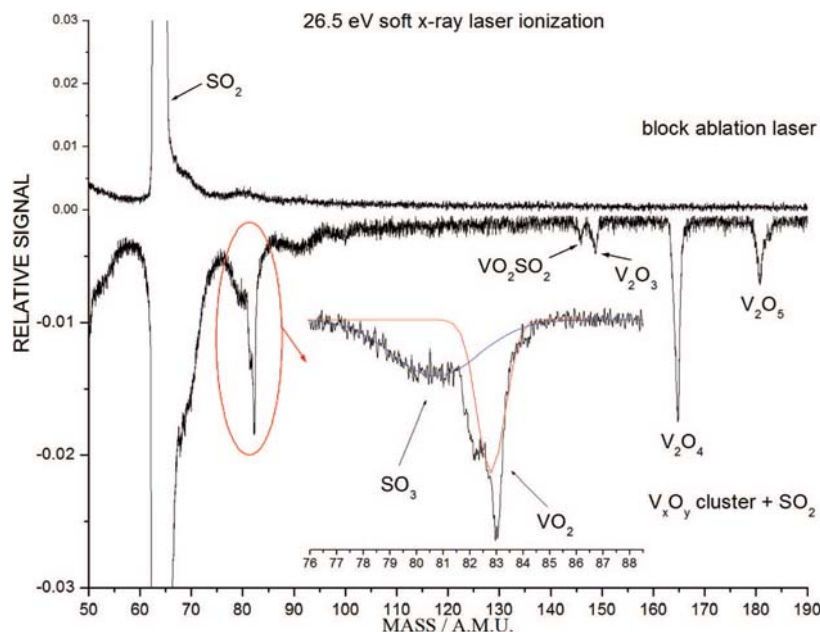
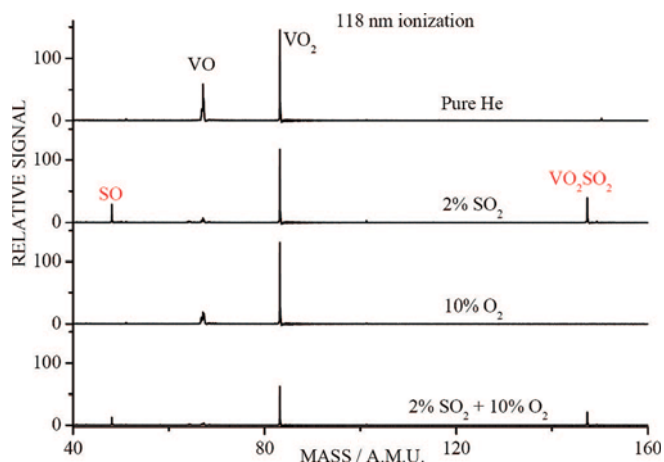


Figure 6 presents the mass spectrum obtained for reactions of  $V_mO_n$  clusters with  $SO_2$  employing the 26.5 eV soft X-ray laser for ionization. A mass peak at 80 amu ( $SO_3$ ) is detected if  $SO_2$  is added to the fast-flow reactor, as shown in the bottom spectrum. If the ablation laser is blocked to prevent the generation of  $V_mO_n$  clusters, the  $SO_3$  signal disappears along with the cluster signals (e.g.,  $V_2O_4$ ), as shown in the top spectrum. The ionization energy of  $SO_3$  is measured to be 13.15 eV.<sup>34</sup> A 118 nm laser is not able to ionize  $SO_3$





**Figure 6.** TOF mass spectra for reaction of  $V_mO_n$  with  $SO_2$  employing a 26.5 eV soft X-ray laser for ionization. A product  $SO_3$  is observed when  $SO_2$  is added (bottom trace), and it disappears with the  $V_mO_n$  cluster signal when the ablation laser is blocked (top trace).



**Figure 7.** TOF mass spectra (low-mass region) for reactions of  $V_mO_n$  with 2%  $SO_2$  (top second trace), 10%  $O_2$  (top third trace), and 2%  $SO_2$ /10%  $O_2$  mixed (bottom trace) gases. A reference spectrum with no  $SO_2$  or  $O_2$  added in the reactant gas channel (pure He is used) is shown in the top trace.

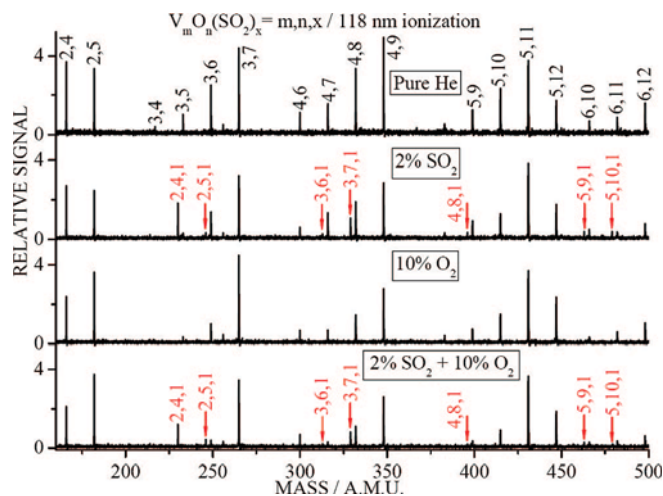


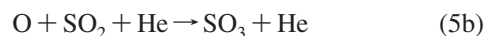
**Figure 8.** TOF mass spectra (high-mass region) for reactions of  $V_mO_n$  with 2%  $SO_2$  (top second trace), 10%  $O_2$  (top third trace), and 2%  $SO_2$ /10%  $O_2$  mixed (bottom trace) gases. A reference spectrum with no  $SO_2$  or  $O_2$  added in the reactant gas channel (pure He is used) is shown in the top trace.

through single-photon ionization, and the X-ray laser is an essential tool for the detection of this product. From the bottom trace of the Figure 6, two obvious bumps are observed and overlapped with the predicted  $SO_3$  signal around 80–100 amu: the explanation for these features and their probable assignments will be presented in the Discussion.

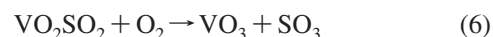
Results for the addition reactions of  $V_mO_nSO_2$  association products with  $O_2$  are shown in Figures 7 and 8 for the low- and high-mass regions, respectively. Interpretation of the data is complicated by reaction of  $V_mO_n$  with  $O_2$  because a signal decrease of the oxygen-deficient clusters, such as VO,  $V_3O_5$ , and  $V_4O_{6-8}$ , due to the presence of  $O_2$ , is clearly observed in comparison to  $VO_2$ ,  $V_3O_7$ , and  $V_4O_9$  features.

The spectra in Figure 7 show that if  $SO_2/O_2$  mixtures rather than  $SO_2$  are used as reactant gases, a big signal decrease of SO,  $VO_2$ , and  $VO_2SO_2$  is observed (compare the spectrum in the bottom trace with the one in the top second trace). Decrease of SO signal intensity can be interpreted in terms of two processes: oxygen-deficient clusters (such as VO,

$V_3O_5$ ,...) react with  $O_2$  so that reactions 1 and 4 produce less SO, and SO produced from reactions 1 and 4 reacts with  $O_2$ :<sup>35,36</sup>



Decrease of  $VO_2$  and  $VO_2SO_2$  signal intensity can also be interpreted as due to two processes: (A) VO reacts with  $O_2$  (to form  $VO_3$ , not detectable by 118 nm laser single-photon ionization,  $IE(VO_3) > 10.5$  eV)<sup>21</sup> so that reactions 1 and 2 produce less  $VO_2$  and  $VO_2SO_2$ , respectively; and (B) fully or partially stabilized  $VO_2SO_2$  from reaction 2b reacts with  $O_2$ , to yield



The rate for reaction 2b is dependent upon the cooling efficiency of collisions with He in the fast-flow reactor; that is,

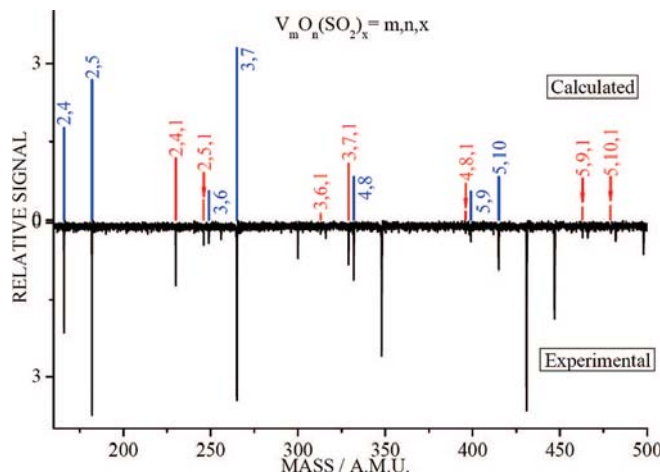


**Figure 9.** Top trace: calculated mass spectra for selected mass peaks using the top three spectra in Figure 8.  $V_mO_n$  signal intensities are calculated by considering the reaction of  $V_mO_n$  with 10%  $O_2$  followed by further reaction with 2%  $SO_2$  (using the relative signal change for  $V_mO_n$  clusters in the top second trace with respect to the top trace in Figure 8).  $V_mO_nSO_2$  signal intensities are calculated using a fixed intensity ratio of  $V_mO_nSO_2$  to  $V_mO_n$  in the top second trace in Figure 8. Bottom trace: replot of TOF spectrum shown by the bottom trace in Figure 8.

$VO_2SO_2^*$  must be stabilized by collisional cooling. As seen from the third trace of Figure 7,  $VO_2$  does not react with  $O_2$ , so that the decrease of the  $VO_2$  signal in the bottom trace of Figure 7 is only due to the reaction of  $VO_2 + SO_2 \rightarrow VO_2SO_2$ . On the basis of the spectra presented in Figure 7, one can suggest reaction 6 is faster than reaction 2b.

The depletion of VO by 2%  $SO_2$  is significantly larger than that by 10%  $O_2$  (compare the top second and third traces in Figure 7 for VO peak), indicating that the rate of reaction  $VO + O_2$  is slower than the rate of reaction  $VO + SO_2$ . This rate difference implies that process A above may not be the main cause of the  $VO_2$  and  $VO_2SO_2$  signal decrease when  $O_2$  is further mixed with  $SO_2$ . As a result, reaction 6 is a possible process that occurs in the fast-flow reactor. In Figure 8,  $V_2O_4SO_2$  (2,4,1),  $V_3O_7SO_2$  (3,7,1), and  $V_5O_{10}SO_2$  (5,10,1) signal decreases are also evident if  $SO_2$  is further mixed with  $O_2$ . This implies similar oxidation reactions to that given in eq 6 may also occur for these association products, although  $O_2$  itself can cause signal changes for vanadium oxide clusters (such as  $V_2O_4$ ,  $V_3O_7$ , and  $V_5O_{10}$ ). The top trace of Figure 9 plots simulated signal intensities for clusters and association products under conditions of cluster reactions with 2%  $SO_2 + 10\% O_2$ , by using the data depicted in the top three spectra of Figure 8 [i.e., (pure He spectrum) + (change made by 2%  $SO_2$ ) + (change made by 10%  $O_2$ )]. In this simulation, cross-reactions, such as oxidation of association products by  $O_2$  (as in reaction 6) are not taken into account. The bottom trace replots the bottom spectrum in Figure 8. Note that the simulated signals for  $V_3O_7SO_2$  and  $V_5O_{10}SO_2$  are significantly more intense than the observed signal, indicating that  $V_3O_7SO_2$  and  $V_5O_{10}SO_2$  may be further oxidized by  $O_2$  in the fast-flow reactor.

#### IV. Discussion

The major and new experimental and theoretical finding for these studies is the detection and prediction of the presence of SO in the reaction of  $SO_2$  with neutral  $V_mO_n$  clusters. As we show below in section IVA, this generation of SO from  $SO_2$  is much more favorable for neutral  $V_mO_n$  clusters than for cationic or anionic  $V_mO_n^\pm$  clusters. In addition, the possibility of back-

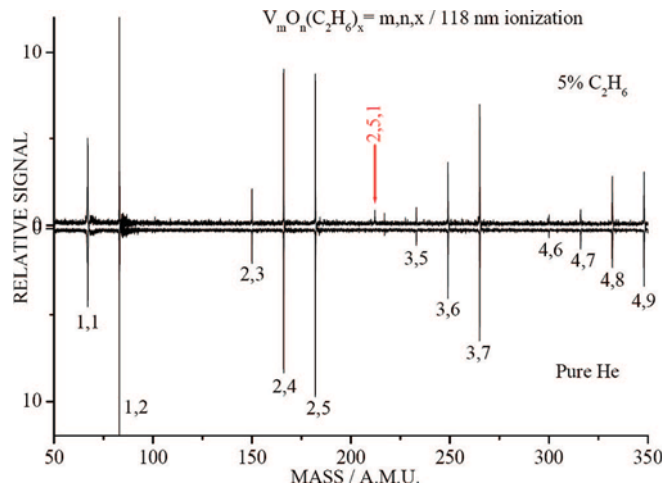


**Figure 10.** TOF mass spectra for interactions of  $V_mO_n$  with 5%  $C_2H_6$  seeded in He (top trace) and pure He (bottom trace).

flow of the reactant gases ( $SO_2$ ,  $SO_2/O_2$ ) into the cluster formation region is discussed and excluded below in section IVB. These are important points because they further support the neutral and preformed cluster origin of the reported chemistry. Possible direct detection of  $SO_3$  is also discussed below in section IVC. The temperature issue for observing the reactivity of  $V_mO_n$  and the rate constants of  $V_mO_n + SO_2$  reactions are discussed below in section IVD. The support of the experimental results by theoretical computations is discussed below in section IVE. The final section (IVF) of this discussion presents possible correspondences between the present gas-phase reactions and condensed-phase reaction mechanisms for the catalytic conversion of  $SO_2$  to  $SO_3$  in the presence of  $V_2O_5$  and  $O_2$ .

##### A. Charge-Transfer Concern in the Fast-Flow Reactor.

Neutral, cationic, and anionic particles are all generated from laser ablation and can react with the  $SO_2$  in the fast-flow reactor. An electric field is inserted after the reactor in order to deflect ions from the molecular beam; thus, the question of charge transfer or neutralization in the reactor is addressed, since these reactions will distort the experimental results for the pure neutral cluster reactions. Exclusion of neutral product formation by ion-molecule reactions in the fast-flow reactor is difficult; however, the following experimental and calculational evidence supports the neutral cluster origin of all the observed reactions.

First, the chemistry of the neutral metal oxide clusters and anionic/cationic metal oxide clusters is obviously different. For example, the cluster distribution of cationic  $V_mO_n^+$  is essentially different from the distribution of neutral  $V_mO_n$ .  $V_2O_4-8^+$ ,  $V_3O_6-9^+$ , and  $V_4O_8-12^+$  species are observed as dominant in the ionic cluster distribution,<sup>37</sup> while  $V_2O_3-6$ ,  $V_3O_6-8$ , and  $V_4O_8-10$  are detected in the neutral distribution.<sup>26</sup> If charge transfer occurs in the fast-flow reactor, we should observe oxygen-rich clusters, such as  $V_2O_7-8$ ,  $V_3O_9$ , and  $V_4O_{11-12}$ , after neutralization of cationic species in collisions with neutral clusters and other species; however, this is not the case for the present experiments.

Second, from signal decrease for reactant clusters ( $V_mO_n$ ) accompanying the comparable signal increase for products ( $V_mO_nSO_2$ ) in Figures 2, 4, and 5, one can conclude that the dominant contribution to the appearance of neutral products is from neutral cluster reactions. Moreover, the mass spectra presented in Figure 10 show that the signal intensity for  $V_mO_n$  does not decrease if  $C_2H_6$  is seeded with the bath gas. Since  $V_mO_n^+$  react with  $C_2H_x$  ( $x = 4, 6$ ),<sup>38</sup> one can conclude that only

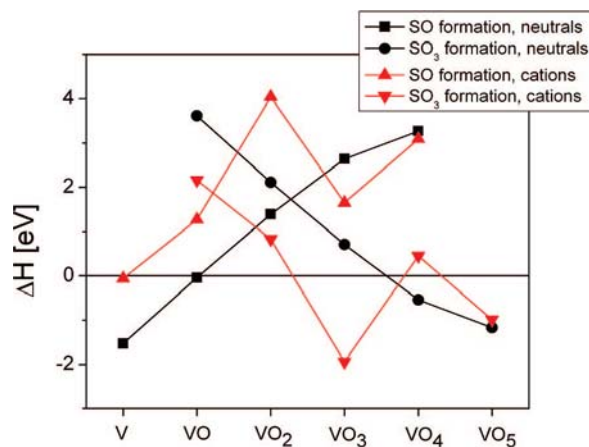


**Figure 11.** Enthalpy (at 298.15 K) for  $\text{VO}_n^{0/+} + \text{SO}_2 \rightarrow \text{VO}_{n+1}^{0/+} + \text{SO}$  and  $\text{VO}_n^{0/+} + \text{SO}_2 \rightarrow \text{VO}_{n+1}^{0/+} + \text{SO}_3$  reactions.

a little  $\text{V}_m\text{O}_n^+$  is present in the ablation source relative to the neutral concentration. The ratio of ionic species to neutral species in typical ablation sources is expected to be  $10^{-2}$  to  $10^{-3}$  on the basis of qualitative estimates and experimental results.<sup>39</sup> Such results strongly imply that the  $\text{V}_m\text{O}_n/\text{SO}_2$  reactions displayed in Figures 2, 4, and 5 are consistent with neutral  $\text{V}_m\text{O}_n$  chemistry. Note that the reactivity of  $\text{V}_m\text{O}_n^-$  is less than that of  $\text{V}_m\text{O}_n^+$ .<sup>38</sup>

Third, one can increase the fast flow reactor tube diameter and thereby reduce the probability of charge-transfer reactions between charged and neutral species. Such studies for  $\text{Nb}_n^{0, \pm}$  and  $\text{Fe}_n^{0,+}$  clusters find negligible effect for the individual cluster distributions, and charged clusters apparently do not influence the neutral cluster chemistry.<sup>40,41</sup> A possible reason for negligible ion–molecule reaction effect on neutral cluster reactivity is that many more neutral clusters than ionic clusters are present after the cluster growth process, especially in the case in which the experimental conditions are optimized to produce the neutral clusters as efficiently possible.<sup>39</sup>

Fourth, we can reduce the number of charged particles entering the fast-flow reactor by as much as 60% (through an electric field inserted between the cluster generation channel and fast-flow reactor) and find no change in the neutral cluster or product distribution.

Fifth, SO formation on neutral  $\text{V}_m\text{O}_n$  clusters is thermodynamically more favorable than on the related cationic clusters. The reaction enthalpies for  $\text{VO}_n + \text{SO}_2$  and  $\text{V}_2\text{O}_n + \text{SO}_2$  are calculated by BPW91/LANL2DZ density functional theory coupled with experimental correction and presented in Figures 11 and 12.<sup>28</sup> As seen from Figures 11 and 12, isolated  $\text{SO}_3$  product generation is favorable both on neutral  $\text{VO}_4$ ,  $\text{VO}_5$ ,  $\text{V}_2\text{O}_6$ , and  $\text{V}_2\text{O}_7$  clusters and ionic  $\text{VO}_3^+$ ,  $\text{VO}_5^+$ ,  $\text{V}_2\text{O}_5^+$ , and  $\text{V}_2\text{O}_6^+$  clusters; however, SO formation is only favorable on neutral clusters, V,  $\text{V}_2\text{O}_2$ , and  $\text{V}_2\text{O}_3$ . Observation of the isolated SO signal in Figures 2 and 7 strongly suggests that contributions from ions in the fast flow reactor experiments are negligible.

**B. Back-Flow Concern in the Fast-Flow Reactor.** One may argue that a possible problem with the experimental setup shown in Figure 1 to investigate neutral cluster reactivity is the direct coupling of the fast-flow reactor to the cluster formation channel: Such connection might enable back-flow of the reactant gases ( $\text{SO}_2$ ,  $\text{SO}_2/\text{O}_2$ ) into the cluster formation region, and, as a result, the laser ablation generated plasma could react with reactant gases directly and the original cluster distribution could be changed.

To address this concern, saturated hydrocarbons, such as  $\text{C}_2\text{H}_6$  instead of  $\text{SO}_2$ , are used as the reactant gas. The result is shown

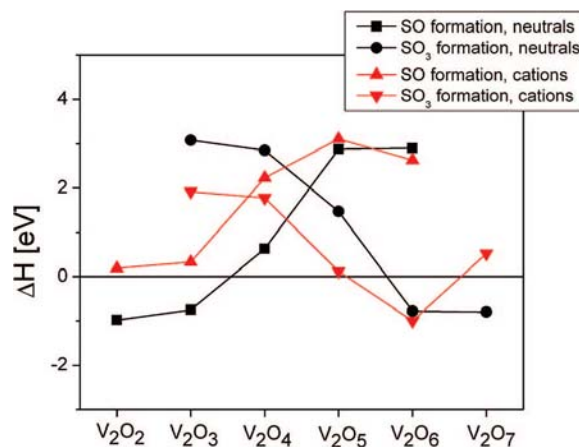


**Figure 12.** Enthalpy (at 298.15 K) for  $\text{V}_2\text{O}_n^{0/+} + \text{SO}_2 \rightarrow \text{V}_2\text{O}_{n+1}^{0/+} + \text{SO}$  and  $\text{V}_2\text{O}_n^{0/+} + \text{SO}_2 \rightarrow \text{V}_2\text{O}_{n+1}^{0/+} + \text{SO}_3$  reactions.

in Figure 10. Considering about 10% experimental uncertainty for mass peak intensities and the weak association reaction between  $\text{V}_2\text{O}_5$  and  $\text{C}_2\text{H}_6$ , the presence of  $\text{C}_2\text{H}_6$  in the fast-flow reactor essentially causes no change of the cluster distribution. We do observe change of selective depletion of  $\text{V}_m\text{O}_n$  clusters and association products if unsaturated hydrocarbons, such as  $\text{C}_2\text{H}_2$  and  $\text{C}_2\text{H}_4$ , are used. This result can be well-interpreted as reactions of  $\text{V}_m\text{O}_n$  with the reactant gas molecules ( $\text{C}_2\text{H}_2$  and  $\text{C}_2\text{H}_4$ ) in the fast-flow reactor. The details are presented in a separate publication.<sup>33</sup> Hydrocarbons, such as methane and others, are extensively used as carbon sources to produce metal carbides by reaction with laser ablation generated metal (Ti, Zr, V, Nb,...) plasmas.<sup>42</sup> Thus, essentially no change of the  $\text{V}_m\text{O}_n$  distribution caused by  $\text{C}_2\text{H}_6$  as shown in Figure 10 implies that reactant gas back-flow is not a problem in our experiments. If back-flow into the cluster formation region were a problem,  $\text{C}_2\text{H}_6$  would react strongly with vanadium plasma to produce vanadium carbides or at least change the original oxide cluster distribution if  $\text{C}_2\text{H}_6$  gas spatially overlaps with the plasma. So we conclude that the present reactions arise from preformed vanadium oxide clusters with the reactant gases in the fast-flow reactor. One may additionally argue that due to residual  $\text{SO}_2$  in the vacuum system, the surface of the used metal (V) foil can absorb  $\text{SO}_2$  that eventually results in production and observation of sulfur-containing clusters  $\text{V}_m\text{O}_n\text{SO}_2$ . Because signals of  $\text{V}_m\text{O}_n\text{SO}_2$  disappear while signals of  $\text{V}_m\text{O}_n$  increase (due to no scattering) immediately after closing nozzle II in the experiment, the  $\text{SO}_2$  adsorption is not a problem. In other words, the results of the “pure He” spectra in Figures 2, 4, and 5 can be reproduced no matter when the spectra are recorded: before, between, or after the recording of the other spectra with  $\text{SO}_2$  injected.

**C. Observation of  $\text{SO}_3$  by X-Ray Ionization.** In the  $\text{V}_m\text{O}_n + \text{SO}_2$  reaction, a mass peak at 80 amu is detected by 26.5 eV ionization as shown in Figure 6. The intensity of this signal is related to the generation of  $\text{V}_m\text{O}_n$  clusters: when the ablation laser is blocked, meaning no  $\text{V}_m\text{O}_n$  clusters are generated, the 80 amu signal significantly decreases; however, the 80 amu signal is much broader than  $\text{V}_m\text{O}_n$  cluster signals, for example,  $\text{VO}_2$ ,  $\text{V}_2\text{O}_4$ , etc., as well as that for SO. The 80 amu feature could be caused by hot molecules of  $\text{SO}_3$ , generated from exothermic reactions between  $\text{V}_m\text{O}_n$  and  $\text{SO}_2$ , or ringing on the MCP’s due to a large  $\text{SO}_2$  signal generated by 26.5 eV laser ionization. To clarify this issue, some experiments are carried out and the assignment of signal of 80 amu is discussed below.

**1. “ $\text{SO}_3$ ” (80 amu) Signal Not Generated from Contamination of  $\text{SO}_2$  Gas.** In the study of neutral  $\text{V}_m\text{O}_n$  clusters reacting with  $\text{SO}_2$ , pure  $\text{SO}_2$  gas is added to the fast-flow reactor by a



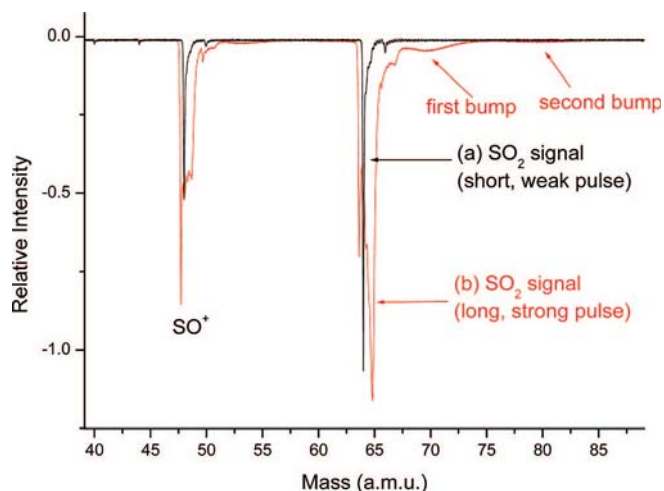


Figure 13. TOF mass spectra for  $SO_2$  added in the fast-flow reactor.

general valve. If a weak  $SO_2$  pulse is employed by adjusting the pulse duration and pulse intensity of the general valve, the MCP detector is not saturated by the  $SO_2$  signal ( $\sim 900$  mV). Using the 26.5 eV laser for ionization, an  $SO_3$  signal is not detected while narrow  $SO$  and  $SO_2$  signals (35 ns) are observed in the mass spectrum.

**2. Signal at 80 amu Not Due to “Ringing” of the MCP Detector.** The line width of the  $SO_2$  signal (Figure 13a) becomes much broader when the pulse intensity and duration of  $SO_2$  gas is increased as shown in Figure 13b. In addition, two obvious “bumps” are observed on the high-mass (right) side of the  $SO_2$  signal. The second bump is located at mass number 80 amu and coincides with the expected  $SO_3^+$  (amu 80) signal. This feature could be caused by the overload of the MCP detector due to too many ions of  $SO_2^+$  generated by 26.5 eV ionization. To avoid the MCP saturation by the  $SO_2^+$  signal, we gate the supplied voltage on the MCP to cut off the  $SO_2^+$  signal. The MCP is gated by simply turning off the bias voltage and then pulsing it on at a specific time after a large, unwanted signal ( $SO_2^+$ , in this case) arrives at the MCP. Nevertheless, the bump at mass number 80 does not disappear while  $SO_2^+$  is completely removed from the mass spectrum; however, the large quantity of ions, generated from the high concentration of reactant in the molecular beam, can adhere to the MCP surface. In other words, the signal species still reaches the detector while the voltage is simply off. The presence of such a large number of ions in a short time on the detector surface may cause a “ringing” response for the detector output because of capacitance issues, arcing, or other reasons, and when the bias voltage is pulsed on, this ringing may be viewed in the mass spectrum and account for the two bumps observed in Figure 6. To address this problem, we use a mass gating technique that does not allow the large number of ions to reach the MCP; thus,  $SO_2^+$  and other large signals in the mass spectrum, such as  $He^+$ ,  $O_2^+$ , and  $Ar^+$ , etc., signals, are reduced to just a few millivolts.

In the present experiments, a reflectron time-of-flight mass spectrometer is used to detect ion signals after the neutral clusters, reactants, and reaction products are ionized by the 26.5 eV soft X-ray laser radiation. The acceleration voltages on the three plates in the ionization region are +1000, +700, and 0 V. A mass gate is placed just before the MCP detector to block selected ions from hitting the detector by pulsing a voltage on the mass gate. A schematic drawing of the mass gate is displayed as Figure 14. The three meshes are evenly spaced over approximately 1 cm, and voltages of 0, 1200, and 0 V are

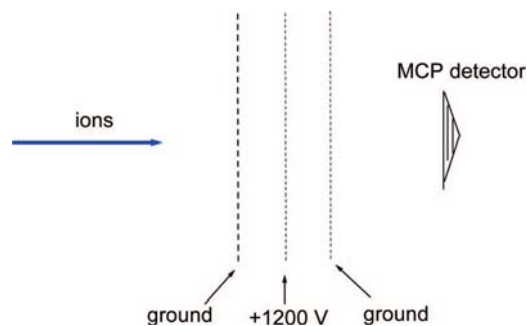


Figure 14. Schematic diagram for the mass gate configuration.

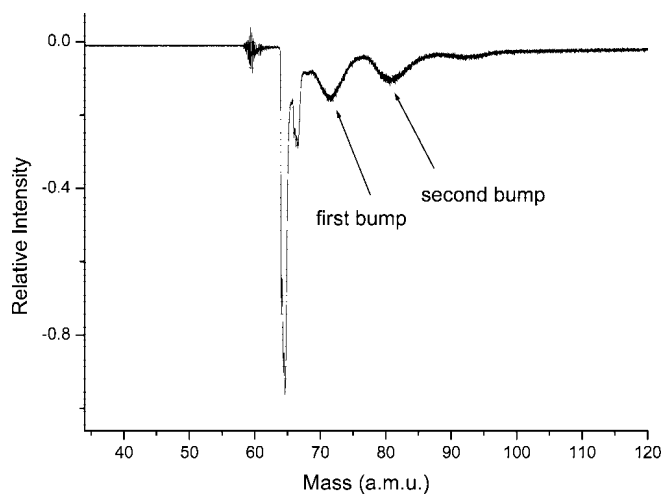


Figure 15. TOF mass spectra for  $SO_2$  with the mass gate configuration.

applied to the three meshes, respectively. The mass gate is enclosed in an aluminum box that is held at ground potential in order to preserve the field-free region of the flight tube. The middle mesh is used as the gate and is pulsed between 0 and 1200 V with a rise and fall time of 25 ns. Ions that are accelerated by 1000 V from the ionization region cannot pass through the mass gate when the voltage of the middle plate is pulsed to 1200 V. The mass gate can block any mass number and any mass region by setting pulse timing and duration parameters for the voltage on the mass gate. Using this design, the shortest pulse duration on the mass gate is measured to be  $\sim 100$  ns; one mass unit up to  $\sim 200$  amu can be selected and blocked from the reacting clusters. In the present experiments, the mass gate is employed to block all the ions less than 70 amu, including the large signals of  $SO_2^+$ ,  $He^+$ ,  $O_2^+$ , and  $Ar^+$ , etc. The advantage of using a mass gate is that the large quantity of ions ionized by the 26.5 eV laser are prevented from arriving at the MCP detector. Any issue caused by MCP overload, or the oscillation of the electrical circuit associated with the MCP, is thereby completely eliminated. As shown in Figure 15, ion signals less than 60 amu have been cut by the mass gate; however, bumps on the mass spectrum are still obviously present even under these conditions if  $SO_2$  is in the reaction cell. Therefore, one can conclude that the bumps following large signals are not caused by MCP overload or ringing of the electrical circuit. For comparison reasons, the reactions of neutral cobalt oxide clusters with  $SO_2$  in the fast-flow reactor under the same conditions as discussed above are further investigated: the same features, including a broad  $SO_2$  mass peak and the following bumps, are again observed in the mass spectra. What causes these bumps is not certain at present. They may be caused by a large number of photoelectrons that are generated from

the ionization of a large number of neutral species (He, O<sub>2</sub>, and SO<sub>2</sub>, etc.) by the 26.5 eV laser. These photoelectrons will have more than 10 eV energy and are energetic enough to ionize most neutral species in the ionization region. Additionally, high concentrations of He, O<sub>2</sub>, and SO<sub>2</sub> species create a large probability for ionization by the photoelectrons. Species ionized by photoelectrons will yield broad TOF mass features because photoelectrons generated from ionization of beam species and perhaps others are not as well localized as the focused laser light. We do not observe such features (“bumps”) between 66 and 82 amu if SO<sub>2</sub> is not present in the beam or fast-flow reactor. The photoelectrons may also generate ground potential fluctuations in the apparatus at these weak signal levels (ca. 1 mV).

**3. SO<sub>3</sub> Product Generated from V<sub>m</sub>O<sub>n</sub> + SO<sub>2</sub> Reactions.** On the basis of our calculations, SO<sub>2</sub> can be oxidized by oxygen-rich vanadium oxide clusters, such as VO<sub>3</sub>, V<sub>2</sub>O<sub>6</sub>, and V<sub>3</sub>O<sub>7</sub>, etc., to generate SO<sub>3</sub> product. We expect to detect an SO<sub>3</sub> signal only by 26.5 eV soft X-ray laser ionization since the ionization energy of SO<sub>3</sub> (13.15 eV) is higher than 10.5 eV; however, the “bump” signals after the huge SO<sub>2</sub> signal seriously interfere with measurement of SO<sub>3</sub> product signal and confuse the SO<sub>3</sub> assignment. Additionally, only a small amount of SO<sub>3</sub> will be generated in the experiment because oxygen-rich clusters are much less prevalent than oxygen-deficient ones (e.g., VO, V<sub>2</sub>O<sub>3</sub>, V<sub>3</sub>O<sub>6</sub>, etc.) and the most stable clusters (e.g., VO<sub>2</sub>, V<sub>2</sub>O<sub>5</sub>, V<sub>3</sub>O<sub>7</sub>, etc.) under the given experimental conditions. For example, the intensity of the VO<sub>3</sub> signal is about 5% of the intensity of the VO<sub>2</sub> or VO signals in the mass spectrum. Therefore, although the SO product signal generated from oxygen-deficient clusters reacting with SO<sub>2</sub> is readily observed in the experiments, the SO<sub>3</sub> product will have a low concentration in the beam and will be much harder to detect. For instance, the ratio of the VO<sub>2</sub>SO<sub>2</sub> signal intensity to VO<sub>2</sub> is about 15% as presented in Figure 6, and if only a 3 mV intensity of the VO<sub>3</sub> signal is observed, the SO<sub>3</sub> signal can be expected to be ca.  $3 \times 15\% = 0.45$  mV. Although an SO<sub>3</sub> product is contributed from oxygen-rich clusters in general, the total signal intensity is still expected at ca. 2 mV because oxygen-rich clusters are a minor component in the molecular beam even for up to 15% O<sub>2</sub> in the helium carrier gas. Therefore, a small SO<sub>3</sub> signal can be buried by the bump ( $\sim 4\text{--}5$  mV) following the SO<sub>2</sub> signal, as discussed above. Note that the feature at 80 amu is much smaller ( $\sim 1$  mV) in the absence of laser ablation. Thus, we must conclude that, under the present experimental conditions, an SO<sub>3</sub> signal cannot be definitively identified, although such a signal is not inconsistent with, or ruled out by, the experimental observations.

**D. Pick Up Cell vs Fast-Flow Reactor Experiments.** The observation of many association products (V<sub>m</sub>O<sub>n</sub>SO<sub>2</sub> in Figures 2, 4, and 5) at near room temperature conditions indicates that reaction barriers for SO<sub>2</sub> approaching V<sub>m</sub>O<sub>n</sub> are quite small. Prior to the present high-pressure, low-temperature fast-flow reactor studies, some effort was devoted to finding reactions of SO<sub>2</sub> with V<sub>m</sub>O<sub>n</sub> in a low-pressure, high-temperature pick up cell experimental setup, such as that successfully used by us to study dehydrogenation of unsaturated hydrocarbons (C<sub>2</sub>H<sub>2</sub>, C<sub>6</sub>H<sub>6</sub>,...) on metal clusters (Nb<sub>n</sub> and Ta<sub>n</sub>).<sup>43</sup> In the pick up cell setup, V<sub>m</sub>O<sub>n</sub>, formed in a supersonic molecular beam, passes through a reaction cell that contains about 1 mTorr pure SO<sub>2</sub> gas. This pressure is continuous and stable compared to the pulsed pressure in the fast-flow reactor. In this instance, association products (or SO) are not identified, although some hard to reproduce, relative signal intensity changes for the clusters are observed, at a signal/noise ratio of ca. 1–2. This comparison implies that the collision rate (cooling and kinetics) is important

for the reactions. In the fast-flow setup, the instantaneous reactant gas pressure (during V<sub>m</sub>O<sub>n</sub> residence in the tube) is estimated<sup>27</sup> to be 14 Torr under our experimental conditions. This ensures that many collisions can occur between the initial association intermediates V<sub>m</sub>O<sub>n</sub>SO<sub>2</sub>\* and the bath (He) or reactant gases, which remove collisional and binding energies from V<sub>m</sub>O<sub>n</sub>SO<sub>2</sub>\*. In a pick up cell, no such stabilization or opportunity for reaction occurs. Moreover, collisions in the expansion do not cool V<sub>m</sub>O<sub>n</sub> clusters (vibrational temperature  $\geq 700$  K)<sup>21</sup> to ca. 300 K before forming V<sub>m</sub>O<sub>n</sub>SO<sub>2</sub>\*. As a result, V<sub>m</sub>O<sub>n</sub>SO<sub>2</sub>\* in the pick up cell setup can quickly dissociate to regenerate reactants V<sub>m</sub>O<sub>n</sub> and SO<sub>2</sub>. Another important difference between the fast-flow and pick up cell setups is that more collisions between V<sub>m</sub>O<sub>n</sub> and SO<sub>2</sub> can be achieved in the fast-flow reactor than in the pick up cell. Under typical conditions of 5% SO<sub>2</sub> in the fast-flow reactor, the partial SO<sub>2</sub> pressure is about 700 mTorr, much higher than the SO<sub>2</sub> pressure ( $\sim 1$  mTorr) in the pick cell. In the pick up cell, the gas pressure has to be low to prevent extensive collisions that will finally destroy the original molecular beam.<sup>44</sup> Moreover, to prevent pressure overload in the mass spectrometer, the pressure in the pick up cell cannot be high because the reactant gas is continuously flowing.

By using the partial SO<sub>2</sub> gas pressure (700 mTorr at 5% SO<sub>2</sub>) and estimated reaction time (50  $\mu$ s), the first-order depletion rate ( $k_1(\text{V}_m\text{O}_n + \text{SO}_2) \equiv k_{m,n}$ , in units of  $10^{-13}$  cm<sup>3</sup> molecule<sup>-1</sup> s<sup>-1</sup>) of V<sub>m</sub>O<sub>n</sub> clusters in Figure 4 can be estimated:  $k_{2,4} = 8.8$ ,  $k_{2,5} = 11.6$ ,  $k_{3,6} = 14.1$ ,  $k_{3,7} = 9.5$ ,  $k_{4,8} = 8.8$ ,  $k_{4,9} = 4.0$ ,  $k_{5,11} = 4.3$ ,  $k_{5,12} = 2.1$ ,  $k_{6,13} = 8.8$ , and  $k_{6,14} = 3.5$ . Because the depletion due to pure scattering is negligible (see Figure 10), the above listed depletion rates can be taken as true reaction rates between V<sub>m</sub>O<sub>n</sub> and SO<sub>2</sub> under the adopted experimental conditions. Thus, 1 mTorr (density  $\sim 3 \times 10^{13}$  molecules/cm<sup>3</sup>) SO<sub>2</sub> in the pick up cell (reaction time  $\sim 100$   $\mu$ s) is not sufficient to cause an observable reaction depletion of V<sub>m</sub>O<sub>n</sub>. For example, the reaction depletion of V<sub>2</sub>O<sub>5</sub> in the pick up experimental conditions is only 0.35% on the basis of the estimated  $k_{2,5} = 11.6 \times 10^{-13}$  cm<sup>3</sup> molecule<sup>-1</sup> s<sup>-1</sup>. The observed V<sub>m</sub>O<sub>n</sub> depletion in these experiments is thus mostly due to the SO<sub>2</sub> scattering.

**E. Theoretical Computations.** Our preliminary density functional theory (DFT) calculations and those expanded in part I<sup>28</sup> also support the experimental results. The calculations are performed using the Gaussian 98<sup>45</sup> and Gaussian 03<sup>46</sup> programs, the BPW91 functional,<sup>47,48</sup> and the LANL2DZ<sup>49</sup> and TZVP<sup>50</sup> basis sets. (see ref 28, part I, for details). Cluster calculations are performed for many spin states and various isomers, typically within 20 eV of the global minimum structure and electronic state.<sup>28</sup> Many different intermediate states for the reaction complexes are also obtained. The calculated binding energies at the BPW91/TZVP level of theory between V<sub>m</sub>O<sub>n</sub> and SO<sub>2</sub> are high (typically around 2–3 eV for most stable V<sub>m</sub>O<sub>n</sub>SO<sub>2</sub> structures). This explains the observation of many association products, because higher binding energies provide more chance for the bath gas (He) to remove collisional and binding energies from the initial association intermediate (V<sub>m</sub>O<sub>n</sub>SO<sub>2</sub>\*).<sup>43</sup> The Gaussian 98 program is used to investigate the reaction of VO with SO<sub>2</sub>. The reaction pathways are followed, and no overall barrier for reaction 1, which is thermodynamically favored by more than 1 eV according to the calculation, is found.<sup>28</sup> Calculations (using Gaussian 03 program) are specifically applied for reaction 2 followed by reaction 6. The results are schematically shown in Figure 16. A large binding energy is found for VO<sub>2</sub> with SO<sub>2</sub>, and the association reaction 2 is facile (with no barrier), in agreement with observations. VO<sub>2</sub>SO<sub>2</sub>



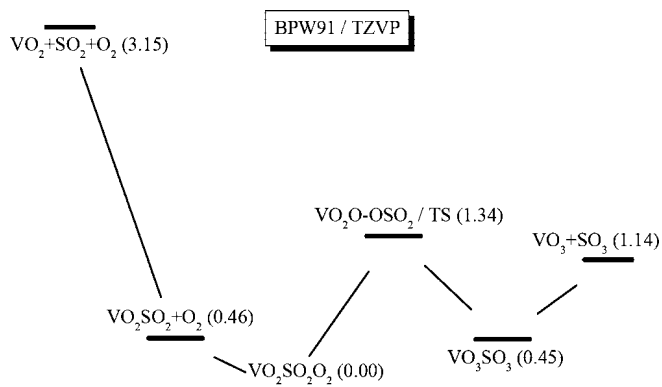


**Figure 16.** Schematic diagram showing  $SO_3$  formation starting from three free gas molecules:  $VO_2$ ,  $SO_2$ , and  $O_2$ . The values in parentheses are relative energies in electronvolts. Note that these calculations are performed with the Gaussian 03 suite of programs and can be different from those of Gaussian 98 by as much as  $\pm 0.05$  eV.

further association with  $O_2$  is also facile, but the association energy is low. A 1.34 eV barrier is determined for the  $VO_2SO_2O_2$  rearrangement to  $VO_3SO_3$ , which essentially involves the breaking of an O–O bond and the making of  $O_2V$ –O and  $O_2S$ –O bonds. The  $SO_3$ – $VO_3$  bond strength is 0.7 eV. The overall reaction  $VO_2 + SO_2 + O_2 \rightarrow VO_3 + SO_3$  is exothermic by 2 eV, but reaction 6 is endothermic by 0.7 eV and has a significant barrier (0.9 eV). Assuming these computed values are relatively accurate, if bath gas collisions do not remove all the collisional and large binding energies present in reaction 2, reaction 5 is quite possible as suggested by the experiment. Thus, this reaction channel is open if bath gas cooling is slower than reaction 6. Note that in general these calculations are probably correct within  $\pm 1$  eV. Further discussion of additional calculation results is presented in part I.<sup>28</sup> Taking account that SO is observed as an isolated product by single-photon ionization (Figure 2), these calculational results also indicate that SO formation is thermodynamically favorable on neutral oxygen-deficient  $V_mO_n$  ( $m = 1, 2, 3, 4$ ) cluster surfaces<sup>28</sup> but unfavorable on all the cationic  $V_mO_n^+$  ( $m = 1, 2$ ) clusters (see Figures 11 and 12). These calculations indicate that SO comes from neutral cluster reactions  $V_mO_n + SO_2 \rightarrow V_mO_{n+1} + SO$  rather than  $V_mO_n^+ + SO_2 \rightarrow V_mO_{n+1}^+ + SO$ . Therefore, the theoretical calculations are in good agreement with experimental observations.

**F. Possible Condensed Phase Reaction Mechanisms.** The present gas-phase studies suggest several molecular level  $SO_3$  formation mechanisms for condensed-phase reactions using vanadium oxides as catalysts: (M1) SO may be formed from oxygen-deficient sites by processes similar to reactions 1 and 4, as suggested by our experiments and calculations— $SO_3$  is formed from reaction of SO with  $O_2$  (reaction 5); (M2)  $SO_3$  may be formed from oxygen-rich sites directly, as our calculations suggest that reactions of oxygen-rich clusters (such as  $V_2O_6$ ,  $V_3O_8$ , and  $V_4O_{11}$ ,...) with  $SO_2$  to form  $SO_3$  are thermodynamically favorable;<sup>28</sup> and (M3)  $SO_3$  formation involves  $SO_2$  association with active sites, followed by oxidation with adsorbed or free  $O_2$ . M1 and M2 do not necessarily address the selectivity of oxidation of  $SO_2$  especially in the presence of vanadium oxide catalysts because any oxygen-poor and oxygen-rich metal oxides will tend to reduce  $SO_2$  to SO and oxidize  $SO_2$  to  $SO_3$ . This arises from a consideration of respective M–O, S–O, and O–O bond strengths. These mechanisms make some sense, however, if one considers that many other supported metal oxides such as  $Fe_2O_3$ ,  $Re_2O_7$ ,  $Nb_2O_5$ , and  $WO_3$  are also found to be catalytic for oxidation of  $SO_2$ , although their performance is not as good as to that found for  $V_2O_5$  catalysts.<sup>7,51</sup> M1, M2,

and the catalytic cycles resulting from these mechanisms are studied in greater detail in part I.<sup>28</sup> The results indicate that the activity of a catalyst for the  $SO_2$  oxidation to  $SO_3$  is dependent on many issues: bond energies, reaction barriers, and reaction rates, etc., not only defect sites on a surface. The M3 mechanism may address the activity of  $SO_2$  over vanadium oxide catalysts as opposed to other metal oxides, because the present gas-phase studies indicate that binding between  $SO_2$  and  $V_mO_n$  is strong and further oxidation of the association intermediates only has a medium ( $\sim 1$  eV) barrier, as shown for the simplest example in Figure 16. We have studied the reaction of neutral iron oxide clusters ( $Fe_mO_n$ ) with  $SO_2$  with no observation of any association products, indicating relatively weak binding between  $Fe_mO_n$  and  $SO_2$ , or a high approaching barrier between them. Below, a catalytic cycle for regeneration will be presented that incorporates these initial reactions.

The apparent activation energy for oxidation of  $SO_2$  over a supported vanadium oxide catalyst is determined to be  $21 \pm 2$  kcal/mol ( $= 0.91 \pm 0.09$  eV).<sup>8,51</sup> Considering the fact that  $VO_n$  represents an active site for a supported  $V_2O_5$  catalyst,<sup>6,8,51</sup> the model study shown in Figure 16 may reflect a real mechanism for condensed-phase catalysis; however, the activation energy ( $0.91 \pm 0.09$  eV) is interpreted as  $SO_3$  desorption energy in the condensed-phase studies. The calculated results (Figure 16) indicate that this activation energy may mainly involve O–O bond cleavage for the  $VO_2O$ – $OSO_2$ / $VO_3SO_3$  complex. This gas-phase interpretation also agrees with the mechanism for oxidation of CO by  $O_2$  over iron oxides: weakening of the O–O bond is a key step.<sup>52</sup>

A “strong support effect” is found for oxidation of  $SO_2$  over supported vanadia catalysts: for example, catalysts supported on a  $CeO_2$  surface are much more reactive than those on a  $SiO_2$  surface.<sup>6</sup> The molecular level effect/mechanism of supports is not well understood due to complexity in the condensed-phase studies.<sup>3,6</sup> A support can certainly modify or change the chemical or electronic properties, and even structures of the supported vanadium oxides, and thereby generate “the support effect”. Molecule level consideration suggest that even the properties of vanadium oxides are little changed by the support; we may still observe the support effect due to reaction kinetics. As implied in Figure 16, reactions 2 and 6 can occur, but bath gas (He) cooling has to be efficient enough to remove energy from the initial association intermediate ( $VO_2SO_2^*$ ). This cooling must be slow enough, however, so that part of the collisional and binding energies between  $VO_2$  and  $SO_2$  remain in the intermediate to overcome the barriers for the processes to form  $VO_3$  and  $SO_3$ . In the condensed phase, controlling collisional and binding energies between supported  $V_mO_n$  and  $SO_2$  is mediated by both surface phonons and reactant gases ( $SO_2/O_2$ ). The cooling rate for surface phonons and reactant gases has to be just right so that processes similar to reactions 2 and 6 can proceed. This provides a new alternative explanation of the support dependence in condensed-phase systems, as different supports should provide different molecular level cooling (vibrational energy redistribution) effects. The experiments and calculations firmly indicate that  $SO_2$  association with most of the neutral vanadium oxide clusters is facile; this association indicates that a vanadium oxide catalyst is potentially useful for  $SO_2$  oxidation because a catalyst should be able to coordinate the molecule that is going to be catalyzed.

The effect of energy dissipation on the surface for catalyst reactivity has never been carefully considered; the phenomenon should be considered if one wants to interpret catalysis at a molecular level. The support effect in catalysis can be very

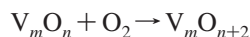
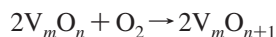
complex, such as change/modification of electronic and geometrical structure of the supported catalyst, change/modification of the structural stability, catalyst acidity and basicity, surface mobility of the supported catalyst, the increase/decrease of the number of active sites of the catalyst, and anything that can change the reaction barriers and yields; however, at a molecular level, energy flow and redistribution within a reaction system has to be considered to interpret mechanisms of a reaction fully, including a catalytic reaction. The major point emphasized by calculations<sup>28</sup> and strongly supported by these experimental results is that the catalytic action of  $V_mO_n$  is based on the thermodynamics of  $SO_2/V_mO_n$  bond strengths and not on reaction barriers modified by special site-specific species.<sup>28</sup>

Moreover, oxygen exchange between  $V_2O_5$  catalyst and their supports can supply more defect sites, oxygen-rich/oxygen-deficient, on the catalyst's surface. In this study, we find that oxidation and reduction of  $SO_2$  can occur on oxygen-rich and oxygen-deficient sites, respectively, for the overall reaction of  $SO_2$  with  $V_mO_n$  clusters.

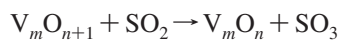
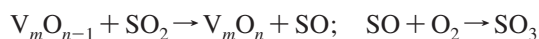
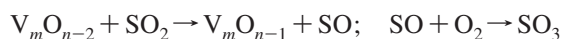
The above-discussed  $SO_3$  formation mechanisms M1 and M2 have as a basic idea that both oxidation and reduction occur for generation of  $SO_3$  from  $SO_2$  assisted by a vanadium oxide catalyst. One of the main advantages of this type of mechanism is that it provides a "catalytic cycle" (regeneration) for the reaction. The following reactions are all possible and form three possible catalytic cycles based on M1–M3 mechanisms of  $SO_3$  formation given above. Note that in the following reactions  $V_mO_n$  is used to describe a stable site.

CATALYTIC CYCLE I: SO and  $SO_3$  formation occur on oxygen deficient and oxygen rich sites, respectively.

1. Formation of oxygen-deficient and oxygen-rich sites

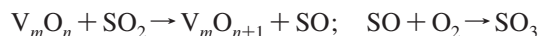
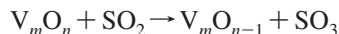


2. Reactions of oxygen-deficient and oxygen-rich sites with  $SO_2$  and regeneration:

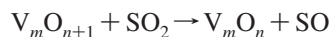
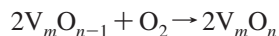
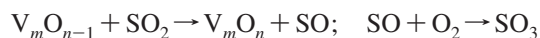


CATALYTIC CYCLE II: SO and  $SO_3$  formation occur on stable sites.

1. Reactions of stable sites with  $SO_2$ , formation of oxygen-rich and oxygen-deficient sites:

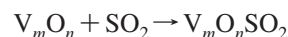


2. Regeneration of stable sites:

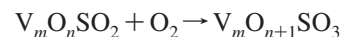


CATALYTIC CYCLE III:  $SO_3$  formation occurs on stable sites through oxidation by both  $O_2$  and catalyst.

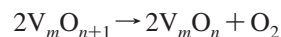
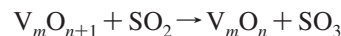
1. Formation of reaction intermediate from a stable site:



2. Oxidation of a reaction intermediate by  $O_2$  and  $SO_3$  formation:



3. Regeneration of a stable site:



Thus, even though we do not study the full catalytic cycle of the condensed phase, gas-phase cluster chemistry can be employed to suggest such mechanistic processes based on observed cluster behavior and calculated mechanisms. We do not necessarily support or emphasize any one of these above mechanisms in particular: all seem possible and may well be simultaneously active or separately active under experimental conditions.

## V. Conclusions

Due to fragmentation found for multiphoton or electron impact ionization processes, neutral cluster reactivity has been previously difficult to access and assess. In this work, the technique of single-photon ionization is successfully employed to study the reactivity of neutral vanadium oxide clusters toward sulfur dioxide in the gas phase. Many association reaction intermediates  $V_mO_nSO_2$ , as well as reaction products SO and  $SO_3$ , are observed. Both experiments and calculations suggest that  $SO_2$  can be reduced and oxidized by oxygen-deficient and oxygen-rich clusters, respectively. Further reactions of  $VO_2SO_2$ ,  $V_3O_7SO_2$ , and  $V_5O_{10}SO_2$  with  $O_2$  are positively identified. Three  $SO_3$  formation mechanisms (M1–M3, see Discussion) are proposed. Several condensed-phase catalytic cycles are suggested on the basis of these  $SO_3$  formation mechanisms. At the molecular level, the importance of catalyst supports is considered to be at least associated with cooling of the active site based on observations of gas-phase reactivity for pick up cell (high-temperature) and fast-flow reactor (low-temperature) experiments. Gas-phase collisions and cooling by surface phonons appear as unavoidable features for these reactions. A full understanding of oxidation of  $SO_2$  over vanadia catalysts needs further studies of both gas- and condensed-phase systems. Results of the present gas-phase study provide new ideas/mechanisms, such as intermediates (SO,  $V_mO_nSO_2$ ) and oxidation of the intermediates, that may be observed and checked in investigations of the condensed-phase systems.

**Acknowledgment.** This work was supported by Philip Morris, U.S.A., the U.S. DOE BES program, and the NSF ERC for Extreme Ultraviolet Science and Technology under NSF Award No. 0310717.

## References and Notes

- (1) Ertl, G.; Knozinger, H.; Weikamp, J. *Handbook of Heterogeneous Catalysis*; Wiley-VCH: Weinheim, Germany, 1997.
- (2) Horvath, I. T. *Encyclopedia of Catalysis*; Wiley: New York, 2003.
- (3) Weckhuysen, B. M.; Keller, D. E. *Catal. Today* **2003**, 78, 25.
- (4) Fierro, J. L. G. *Metal Oxides*; Taylor & Francis: London, 2006.
- (5) van Santen, R. A.; Neurock, M. *Molecular Heterogeneous Catalysis*; Wiley-VCH: Weinheim, Germany, 2006.
- (6) Wachs, I. E. *Catal. Today* **2005**, 100, 79.
- (7) Dunn, J. P.; Stenger, H. G., Jr.; Wachs, I. E. *J. Catal.* **1999**, 181, 233.
- (8) Dunn, J. P.; Stenger, H. G., Jr.; Wachs, I. E. *Catal. Today* **1999**, 51, 301.

- (9) Giakoumelou, I.; Parvulescu, V.; Boghosian, S. *J. Catal.* **2004**, 225, 337.
- (10) van Lingen, J. N. J.; Gijzen, O. L. J.; Weckhuysen, B. M.; van Lenthe, J. H. *J. Catal.* **2006**, 239, 34.
- (11) Keller, D. E.; Koningsberger, D. C.; Weckhusen, B. M. *J. Phys. Chem. B* **2006**, 110, 14313.
- (12) Muetterties, E. L. *Science* **1977**, 196, 839.
- (13) Witko, M.; Hermann, K.; Tokarz, R. *J. Electron Spectrosc. Relat. Phenom.* **1994**, 69, 89.
- (14) Lai, X.; Goodman, D. W. *J. Mol. Catal. A* **2000**, 162, 33.
- (15) Thomas, J. M. *Top. Catal.* **2005**, 38, 3.
- (16) Justes, D. R.; Mitric, R.; Moore, N. A.; Bonacic-Koutecky, V.; Castleman, A. W., Jr. *J. Am. Chem. Soc.* **2003**, 125, 6289.
- (17) Fielicke, A.; Mitric, R.; Meijer, G.; Bonacic-Koutecky, V.; van Helden, G. *J. Am. Chem. Soc.* **2003**, 125, 15716.
- (18) Moore, N. A.; Mitric, R.; Justes, D. R.; Bonacic-Koutecky, V.; Castleman, A. W., Jr. *J. Phys. Chem. B* **2006**, 110, 3015.
- (19) Feyel, S.; Schroder, D.; Rozanska, X.; Sauer, J.; Schwarz, H. *Angew. Chem., Int. Ed.* **2006**, 45, 4677.
- (20) Feyel, S.; Schroder, D.; Rozanska, X.; Sauer, J.; Schwarz, H. *Angew. Chem., Int. Ed.* **2006**, 45, 4681.
- (21) Matsuda, Y.; Bernstein, E. R. *J. Phys. Chem. A* **2005**, 109, 3803.
- (22) Matsuda, Y.; Bernstein, E. R. *J. Phys. Chem. A* **2005**, 109, 314.
- (23) Matsuda, Y.; Shin, D. N.; Bernstein, E. R. *J. Chem. Phys.* **2004**, 120, 4142.
- (24) Shin, D. N.; Matsuda, Y.; Bernstein, E. R. *J. Chem. Phys.* **2004**, 120, 4157.
- (25) Matsuda, Y.; Shin, D. N.; Bernstein, E. R. *J. Chem. Phys.* **2004**, 120, 4165.
- (26) Dong, F.; Heinbuch, S.; He, S.-G.; Xie, Y.; Rocca, J. J.; Bernstein, E. R. *J. Chem. Phys.* **2006**, 125, 164318.
- (27) Geusic, M. E.; Morse, M. D.; O'Brien, S. C.; Smalley, R. E. *Rev. Sci. Instrum.* **1985**, 56, 2123.
- (28) Jakubikova, E.; Bernstein, E. R. *J. Phys. Chem. A* **2007**, 111, 13339.
- (29) Xie, Y.; He, S.-G.; Dong, F.; Bernstein, E. R. *J. Chem. Phys.* **2008**, 128, 044306.
- (30) Shin, D. N.; Matsuda, Y.; Bernstein, E. R. *J. Chem. Phys.* **2004**, 120, 4150.
- (31) Dong, F.; Heinbuch, S.; Rocca, J. J.; Bernstein, E. R. *J. Chem. Phys.* **2006**, 124, 224319.
- (32) Rocca, J. J. *Rev. Sci. Instrum.* **1999**, 70, 3799.
- (33) Dong, F.; Heinbuch, S.; Xie, Y.; Rocca, J. J.; Bernstein, E. R.; Wang, Z.; Deng, K.; He, S.-G. *J. Am. Soc. Soc.* **2008**, 130, 1932.
- (34) Snow, K. B.; Thomas, T. F. *Int. J. Mass Spectrom. Ion Process.* **1990**, 96, 49.
- (35) Black, G.; Sharpless, R. L.; Slanger, T. G. *Chem. Phys. Lett.* **1982**, 90, 55.
- (36) Garland, N. L. *Chem. Phys. Lett.* **1998**, 290, 385.
- (37) Bell, R. C.; Zemski, K. A.; Kerns, K. P.; Deng, H. T.; Castleman, A. W., Jr. *J. Phys. Chem. A* **1998**, 102, 1733.
- (38) Zemski, K. A.; Justes, D. R.; Castleman, A. W., Jr. *J. Phys. Chem. A* **2001**, 105, 10237.
- (39) Bowen, K. Personal communication to E.R.B.
- (40) Zakin, M. R.; brickman, R. O.; Cox, D. M.; Kaldor, A. *J. Chem. Phys.* **1988**, 88, 3555.
- (41) Zakin, M. R.; brickman, R. O.; Cox, D. M.; Kaldor, A. *J. Chem. Phys.* **1988**, 88, 6605.
- (42) Leskiw, B. D.; Castleman, A. W., Jr. *C. R. Phys.* **2002**, 3, 251, and references cited therein.
- (43) He, S.-G.; Xie, Y.; Bernstein, E. R. *J. Chem. Phys.* **2006**, 125, 164306.
- (44) Andersson, M.; Persson, J. L.; Rosén, A. *J. Phys. Chem.* **1996**, 100, 12222.
- (45) Frisch, M. J.; Trucks, G. W.; Schlegel, H. B.; *Gaussian 98*, Revision A.11; Gaussian: Pittsburgh, PA, 2001.
- (46) Frisch, M. J.; Trucks, G. W.; Schlegel, H. B.; *Gaussian 03*, Revision C.02; Gaussian: Wallingford, CT, 2004.
- (47) Becke, A. D. *Phys. Rev. A* **1988**, 38, 3098.
- (48) Perdew, J. P.; Wang, Y. *Phys. Rev. B* **1991**, 45, 13244.
- (49) Hay, P. J.; Wadt, W. R. *J. Chem. Phys.* **1985**, 82, 270.
- (50) Schaefer, A.; Huber, C.; Ahlrichs, R. *J. Chem. Phys.* **1994**, 100, 5829.
- (51) Dunn, J. P.; Stenger, H. G., Jr.; Wachs, I. E. *Catal. Today* **1999**, 53, 543.
- (52) Reddy, B. V.; Rasouli, F.; Hajaligol, M. R.; Khanna, S. N. *Chem. Phys. Lett.* **2004**, 384, 242.

JP805744G